



HAL
open science

Soft-templating synthesis of hierarchical mordenite as highperformance catalyst for cyclic acetals production via acetylation of glycerol and benzaldehyde

Jiang-Tian Gong, Taghrid Alomar, Najla Almasoud, Ludovica Pace, Aurelie Vicente, Pedro Maireles-Torres, Joon Ching Juan, Zeinhom El-Bahy, Svetlana Mintova, Eng-Poh Ng

► To cite this version:

Jiang-Tian Gong, Taghrid Alomar, Najla Almasoud, Ludovica Pace, Aurelie Vicente, et al.. Soft-templating synthesis of hierarchical mordenite as highperformance catalyst for cyclic acetals production via acetylation of glycerol and benzaldehyde. *Microporous and Mesoporous Materials*, 2024, 372, pp.113111. 10.1016/j.micromeso.2024.113111 . hal-04654214

HAL Id: hal-04654214

<https://hal.science/hal-04654214v1>

Submitted on 19 Jul 2024

HAL is a multi-disciplinary open access archive for the deposit and dissemination of scientific research documents, whether they are published or not. The documents may come from teaching and research institutions in France or abroad, or from public or private research centers.

L'archive ouverte pluridisciplinaire **HAL**, est destinée au dépôt et à la diffusion de documents scientifiques de niveau recherche, publiés ou non, émanant des établissements d'enseignement et de recherche français ou étrangers, des laboratoires publics ou privés.

Soft-templating synthesis of hierarchical mordenite as high-performance catalyst for cyclic acetals production via acetylation of glycerol and benzaldehyde

Jiang-Tian Gong,^a Najla AlMasoud,^b Taghrid S. Alomar,^b Ludovica Pace,^c Aurelie Vicente,^c Pedro Maireles-Torres,^d Joon Ching Juan,^e Zeinhom M. El-Bahy,^f Svetlana Mintova,^c Eng-Poh Ng^{a,*}

^a*School of Chemical Sciences, Universiti Sains Malaysia, 11800 USM, Penang, Malaysia.*

^b*Department of Chemistry, College of Science, Princess Nourah bint Abdulrahman University, P.O. Box 84428, Riyadh 11671, Saudi Arabia.*

^c*Normandie University ENSICAEN, UNICAEN, CNRS, Laboratoire Catalyse et Spectrochimie, 14000, Caen, France.*

^d*Departamento de Química Inorgánica Cristalografía y Mineralogía (Unidad Asociada al ICP-CSIC), Facultad de Ciencias Campus de Teatinos, Universidad de Málaga, 29071 Málaga, Spain.*

^e*Nanotechnology & Catalysis Research Centre (NANOCAT), Universiti Malaya, 50603, Kuala Lumpur, Malaysia.*

^f*Department of Chemistry, Faculty of Science, Al-Azhar University, Nasr City 11884, Cairo, Egypt.*

*Corresponding author. Email: epng@usm.my

Abstract

Highly active hierarchical mordenite zeolite with micro/mesoporosity (TM-*n*) for selective synthesis of cyclic acetals *via* acetylation reaction is reported. The hierarchical zeolite is synthesized using soft-templating approach with variations in octadecyltrimethoxysilane (OTMS/Al₂O₃ ratio, *n* = 0.2, 0.3 and 0.4) in precursor hydrogels. The results reveal that OTMS not only creates secondary mesoporosity in zeolite framework (larger mesopore volume, external surface area, average pore diameter), but also influences the crystallization process, altering the crystal morphology, crystallinity and Si/Al ratios. Among TM-*n* zeolites prepared, TM-0.3 hierarchical mordenite has the optimum OTMS amount incorporated while further increasing the OTMS amount leads to the formation of ANA/GIS intergrowth. Thanks to the accessible hierarchical porosity, reduced acidity and morphological effects, the TM-0.3 hierarchical mordenite exhibits excellent catalytic performance (84.1% conversion, TOF = 0.087 s⁻¹, 61.5% dioxolane selectivity) in acetylation of glycerol and benzaldehyde (160 °C, 20 min) better than pristine mordenite. The catalyst is reusable for five runs with minimal loss of activity (TOF = 0.087 → 0.084 s⁻¹), making it a promising catalyst for chemical productions involving bulky molecules. In addition, comparative catalytic tests with classical homogeneous and heterogeneous catalysts, including H₂SO₄, HCl, CH₃COOH, H-Y, H-LTL, Na-X, Na-A, were performed.

Keywords: Hierarchical mordenite; Zeolite; Octadecyltrimethoxysilane; Acetylation of glycerol; Acetal

1. Introduction

Zeolites are crystalline aluminosilicates with uniform microporosity (<2 nm). Zeolites are widely used in catalysis, ion exchange, adsorption and separation due to their high surface area, surface hydrophilicity/hydrophobicity, specific pore size and shape, strong acidity and non-toxicity [1, 2]. To date, more than 250 zeolites with different structural types have been discovered [3].

Mordenite is one of the most important industrial zeolites, particularly in the agriculture and petrochemical sectors [4]. Mordenite has two-dimensional pores ($6.5 \times 7.0 \text{ \AA}^2 \leftrightarrow 2.5 \times 5.7 \text{ \AA}^2$), and this unique pore structure and shape impart excellent adsorption and catalytic properties to mordenite, enabling selective molecular sieving effect [5]. Hence, understanding its unique properties and innovating its synthesis continue to expand its application scope, contributing to further advancements in numerous industries.

However, the microporosity of mordenite limits its application in certain catalytic reactions involving bulky molecules, where the presence of small micropores creates a barrier to molecular diffusion [4]. In addition, the restricted pore size of zeolites can also lead to mass transfer for reactant molecules, causing coking and catalyst deactivation [6]. Hence, various strategies have been employed to address diffusion and mass transfer issues. These approaches encompass enlarging pore size

by disrupting micropore walls *via* post-treatment [7], introducing hierarchical meso/macroporosity (secondary porosity) through hard-templating or soft-templating approaches [8], and downsizing particle size to the nanometer scale [9].

In the post-treatment approach, zeolite is initially synthesized, and then the development of hierarchical mesopores is achieved by selectively leaching the framework atoms (Si or Al) either using acid or fluoride [10–13]. However, these methods possess challenges in controlling the hierarchical mesoporosity and result in partial destruction of the zeolite structure [14].

Another method involves a hard-templating method, where inorganic nanospheres, polymer beads or carbonaceous nanoparticles with well-defined structures are added to impart additional porosity to the zeolite during the synthesis [15]. Nevertheless, this method might face tedious template removal (dissolution, oxidation or combustion) that introduces structural damage or defects [16]. More importantly, achieving precise control over pore size and distribution can be difficult, limiting its feasibility to certain zeolite frameworks.

Recently, Ryoo et al. demonstrated the use of soft-templating method for SAPO-n and zeolite syntheses, by incorporating organosilane surfactants as mesopore-forming agents in the synthesis formulations [17]. These organic supramolecules not only play a role in generating controlled mesoporous systems, but also participate in the overall crystallization process. This method offers advantages in achieving well-defined and controllable mesopore structures, enabling the tailoring of pore sizes and distributions. Despite this, few studies have reported on the synthesis of hierarchical

SAPO and zeolites using organosilanes [18, 19]. Nevertheless, the synthesis of mordenite with hierarchical structure by using this method is scarce thus far.

In this study, a hierarchical mordenite is prepared using soft-templating approach where octadecyltrimethoxysilane (OTMS) acts as a mesoporegen during crystallization process. Furthermore, silica extracted from bamboo leaves is used as a silica source for the synthesis of hierarchical mordenite because it has very high purity of silica and has been proven as a reactive silica in crystallizing various zeolites [20–22]. The resulting hierarchical mordenite exhibits better catalytic performance than classical homogeneous and heterogeneous catalysts in acetylation of glycerol and benzaldehyde under non-microwave instant heating, producing two cyclic acetal products which are useful biofuel additives. We hence believe that the present work would significantly benefit the catalysis research by engineering and developing active hierarchical porous catalysts.

2. Experimental

2.1. Reagents

Nitric acid (HNO_3 , 69%), sodium hydroxide (NaOH pellet, 98%), Ammonium chloride (NH_4Cl , 99.5%), benzaldehyde ($\text{C}_6\text{H}_5\text{CHO}$, 99%) and toluene ($\text{C}_6\text{H}_5\text{CH}_3$, 99.5%) were purchased from Merck. Glycerol (99.5%) was procured from Sigma-Aldrich. Aluminium hydroxide ($\text{Al}(\text{OH})_3$) was obtained from Acros Organics. Octadecyltrimethoxysilane ($\text{C}_{21}\text{H}_{46}\text{O}_3\text{Si}$, 92%) was outsourced from Gelest, Inc. All chemicals were used without further treatment.

2.2. Preparation of bamboo leaves silica (BLA)

The silica was extracted from the bamboo leaves using acid treatment as follows: The bamboo leaves (200 g) were first ground before being soaked in a HNO₃ solution (1.0 M, 48 h). The acid treated leaves were sieved and washed with distilled water until pH 7. The leaves were calcined (600 °C, 5 h) in a furnace and the obtained purely white ash (99.6% SiO₂) was used as silica source in the synthesis of hierarchical mordenite zeolites.

2.3. Synthesis of pristine mordenite

In a typical synthesis, BLA (1.014 g) and NaOH (0.133 g) were dissolved in distilled water (5.333 g) under stirring (95 °C, 2 h). A clear sodium aluminate solution, which was prepared *via* dissolution of Al(OH)₃ (0.129 g) in a NaOH solution (0.552 g, 0.1 M) in an autoclave (170 °C, 5 h), was then added to the silicate solution. Under high pressure (add a value???), the dissolution of Al(OH)₃ was accelerated. The resulting hydrogel of 20SiO₂:1Al₂O₃:3.5Na₂O:388H₂O molar ratio was further stirred (500 rpm, 15 min) before being hydrothermally crystallized in an autoclave (165 °C, 65 h). After cooling down, the solid product was filtered, purified with distilled water to reduce the pH to 7, and dried (80 °C, 12 h). Finally, the Na-mordenite underwent three ion-exchange cycles to convert it to H-mordenite using NH₄Cl (1.0 M) (80 °C, 3 h), followed by calcination (550 °C, 6 h).

2.4. Synthesis of hierarchical mordenites

TM-0.3 sample ($x = 0.3$ is the molar ratio of OTMS) was prepared as follows: Firstly, BLA (1.014 g) were dissolved in an NaOH solution (5.466 g, 0.011 M) at 95 °C (2 h, 400 rpm). The Al(OH)₃ (0.129 g) was also dissolved in an NaOH solution (0.552 g, 0.102 M) in an autoclave (170 °C, 5 h). The resulting clear aluminate solution and octadecyltrimethoxysilane (0.094 g) were subsequently introduced into the silicate solution under agitation (500 rpm, 15 min). The final mixture of 20SiO₂:1Al₂O₃:3.5Na₂O:0.3OTMS:388H₂O was then crystallized (165 °C, 65 h) before the resulting solid product was isolated, purified with distilled water until pH 7, dried (80 °C, 12 h) and calcined (550 °C, 6 h, 1 °C/min). The zeolite sample (5.000 g) was finally converted to the acidic form by successive ion-exchange with NH₄Cl (158.025 g, 1.0 M) thrice before calcination (550 °C, 6 h).

For other TM- x zeolite samples ($x = 0.2, 0.4$), similar synthesis protocol was used but with the addition of different amounts of OTMS (0.063 g and 0.125 g), respectively.

2.5. Characterization

The X-ray diffractograms (XRD) of samples were obtained using a Bruker D8 Avance diffractometer (CuK α , $\lambda = 1.5406 \text{ \AA}$, $2\theta = 4\text{--}40^\circ$, $0.02^\circ/\text{sec}$). The zeolite morphology and size are assessed using a Hitachi Regulus 8220 FESEM microscope.

The IR spectra of framework vibrations were captured using a Perkin Elmer's System 2000 spectrometer where the KBr pelletization technique was used. N₂ adsorption-desorption isotherms were acquired using a Micromeritics ASAP 2010 instrument at -196 °C. Prior analysis, the samples underwent degassing (400 °C, 10 h). The surface areas (specific surface area, micropore surface area, external surface area) were determined using the Brunauer-Emmett-Teller (BET) and t-plot equations. The average pore diameter was calculated with the Barrett-Joyner-Halenda (BJH) method while the total pore volume was calculated using the nitrogen uptake at P/P₀ = 0.98. TGA was performed with a Perkin Elmer TGA7 under air condition. The Si/Al ratio of zeolites was confirmed with a Panalytical Axios Max WDXRF analyzer. The solid-state ²⁹Si MAS NMR spectra were recorded with a Bruker Avance III HD 500 MHz spectrometer at 130.3 MHz through a single-pulse experiment. A 4-mm zirconia rotor was spun at 12 kHz, and the analysis was conducted at a radiofrequency power of 36 kHz. All chemical shifts were referenced to tetramethylsilane. The Si/Al ratio of zeolites was also calculated using the Equation 1 [17]:

$$\text{Si / Al} = \frac{\sum_{n=0}^4 I_{\text{Si} (n\text{Al})}}{\sum_{n=0}^4 (n / 4) I_{\text{Si} (n\text{Al})}} \quad (\text{Equation 1})$$

For NH₃-TPD characterization, the acid density and strength of zeolites were evaluated using a BELCAT-B temperature programmed desorption analyzer probed with NH₃ (TPD-NH₃). The surface of samples was cleaned *via* degassing (400 °C, 5 h) under He flow (30 mL/min), followed saturation with NH₃ for adsorption. The

subsequent step involved the removal of physisorbed NH₃ (30 mL/min) and the NH₃ desorption profile was measured from 50 to 800 °C.

2.6. Acetalization of glycerol and benzaldehyde

The catalytic acetylation of glycerol was examined under non-microwave rapid heating which mimics microwave fast heating [23]. Initially, activated zeolite (0.050 g, 450 °C, 3 h), glycerol (0.200 g) and benzaldehyde (1.612 g) were introduced into a 15-mL glass tube, capped and rapidly heated to 120–160 °C for 0–60 min using a Monowave 50 reactor (Anton Paar). The resulting liquid product was isolated and injected into a GC-FID (Agilent 7890A, HP-5 column) with toluene serving as the internal standard. The conversion and product selectivity were calculated using Equations (2) and (3) [24], respectively:

$$\text{Conversion (\%)} = \left(1 - \frac{[\text{Glycerol}]_t}{[\text{Glycerol}]_0}\right) \times 100 \quad (\text{Equation 2})$$

$$\text{Selectivity (\%)} = \frac{[\text{Dioxolane}]_t \text{ or } [\text{Dioxane}]_t}{[\text{All products}]_t} \times 100 \quad (\text{Equation 3})$$

where [Glycerol]₀ and [Glycerol]_t are the amounts of glycerol at 0 and t min, respectively. [Dioxolane]_t and [Dioxane]_t are the amounts of 2-benzyl-4-hydroxymethyl-1,3-dioxolane and 2-benzyl-5-hydroxy-1,3-dioxane at t min, respectively. The turnover number (TON) and turnover frequency (TOF) were calculated using Equations (4) and (5) [25], respectively:

$$\text{TON} = \frac{n_{\text{product}}}{n_{\text{cat}}} \quad \text{Equations (4)}$$

$$\text{TOF} = \frac{\text{TON}}{t} \quad \text{Equations (5)}$$

where n_{product} is the amount of product (in μmol), n_{cat} is the amount of catalyst (in μmol), t is reaction time (in second).

For catalyst reusability, the solid catalyst after reaction run was soaked and washed with diethyl ether several times before drying at $100\text{ }^{\circ}\text{C}$. The catalyst was activated again ($450\text{ }^{\circ}\text{C}$, 5 h) before being added into the reactants (the amount of reactants used was normalized to the mass of catalyst used), and subjected for the subsequent cycle of catalytic reaction.

3. Results and discussion

3.1. Characterization of porous materials

The crystallinity and purity of samples prepared with different amounts of OTMS are studied by XRD analysis. It is observed that TM-0.2 and TM-0.3 exhibit XRD patterns similar to pristine MOR solid [26] (Fig. 1a–c). No additional XRD peaks from competing phases (e.g. GIS, ANA, SOD) are detected, indicating the absence of competing crystalline solids upon the addition of OTMS mesopore-forming agent. However, the XRD peaks intensity of TM-0.2 and TM-0.3 is lower than that of pristine MOR solid. The degrees of crystallinity for both samples are calculated to be 85.3% and 82.7%, respectively, relative to pristine mordenite. Furthermore, the full width at half

maximum (FWHM) of XRD peaks especially at $2\theta = 6.50^\circ, 9.74^\circ, 25.60^\circ, 26.29^\circ$ for both samples is broadened, indicating the formation of smaller crystallite sizes [27]. Further increasing the OTMS amount to 0.4 (TM-0.4) leads to the formation of ANA/GIS intergrown dense phase (Fig. 1d). Thus, the maximum OTMS/ Al_2O_3 ratio that can be used to synthesize pure hierarchical mordenite is 0.3.

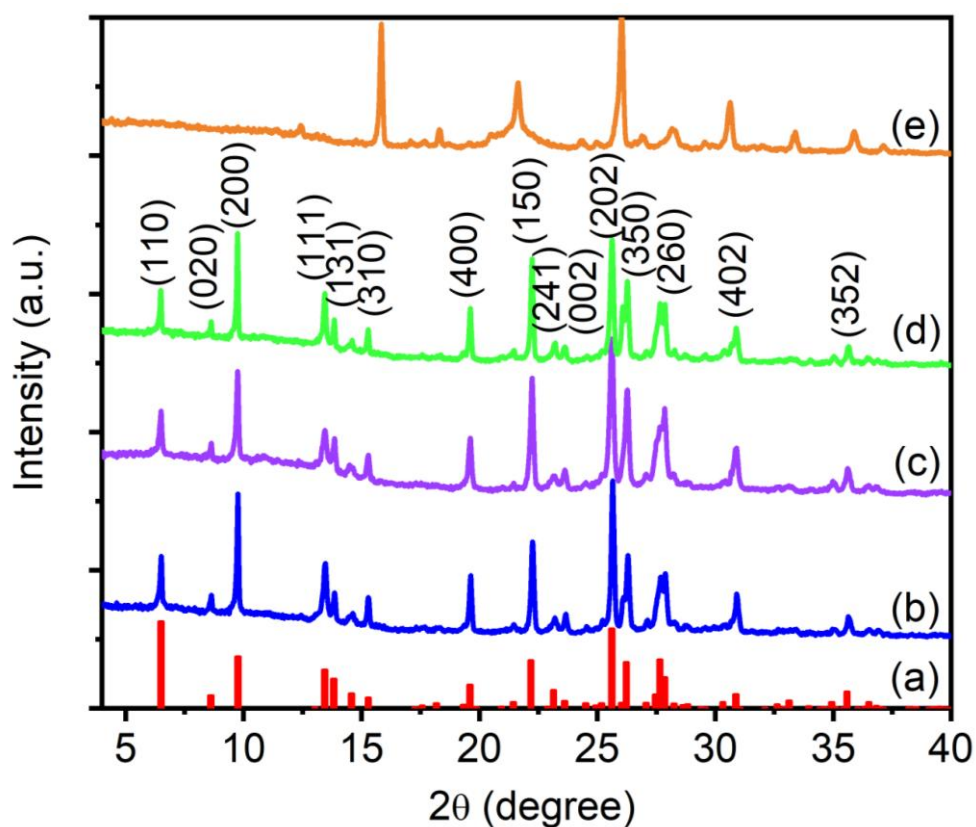


Fig. 1. XRD patterns of (a) simulated mordenite, (b) pristine mordenite, (c) TM-0.2, (d) TM-0.3 and (e) TM-0.4.

The effects of OTMS on morphological properties and chemical composition of mordenites are studied through FESEM and XRF analyses. Pristine mordenite crystals (Si/Al ratio = 6.10) show uniform elongated orthorhombic shape with

dimensions of ca. $3.5 \times 0.3 \times 0.3 \mu\text{m}^3$ (Fig. 2a,b, Table 1) [28]. As the OTMS/ Al_2O_3 ratio increases, the growth on y and z facets is disrupted, resulting in the formation of zeolite crystals with varied morphologies and rough surfaces (Fig. 2c-f). For instance, TM-0.2 forms rectangular bar-like mordenite crystals with an average size of ca. $4.4 \times 0.3 \times 0.1 \mu\text{m}^3$, while TM-0.3, with a higher OTMS amount, displays nano-needle shape (ca. $4.7 \times 0.1 \times 0.1 \mu\text{m}^3$). With an addition of OTMS, an increase in the Si/Al ratio from 6.10 to 6.52 (TM-0.2) and 6.74 (TM-0.3) is also observed where more siliceous framework increases the surface hydrophobicity [29]. TM-0.4 shows a further increase in the Si/Al ratio (7.01) but undergoes a complete change in morphology to an aggregated flower-like feature, further proving the transformation of mordenite crystalline phase to ANA/GIS intergrowth [30].

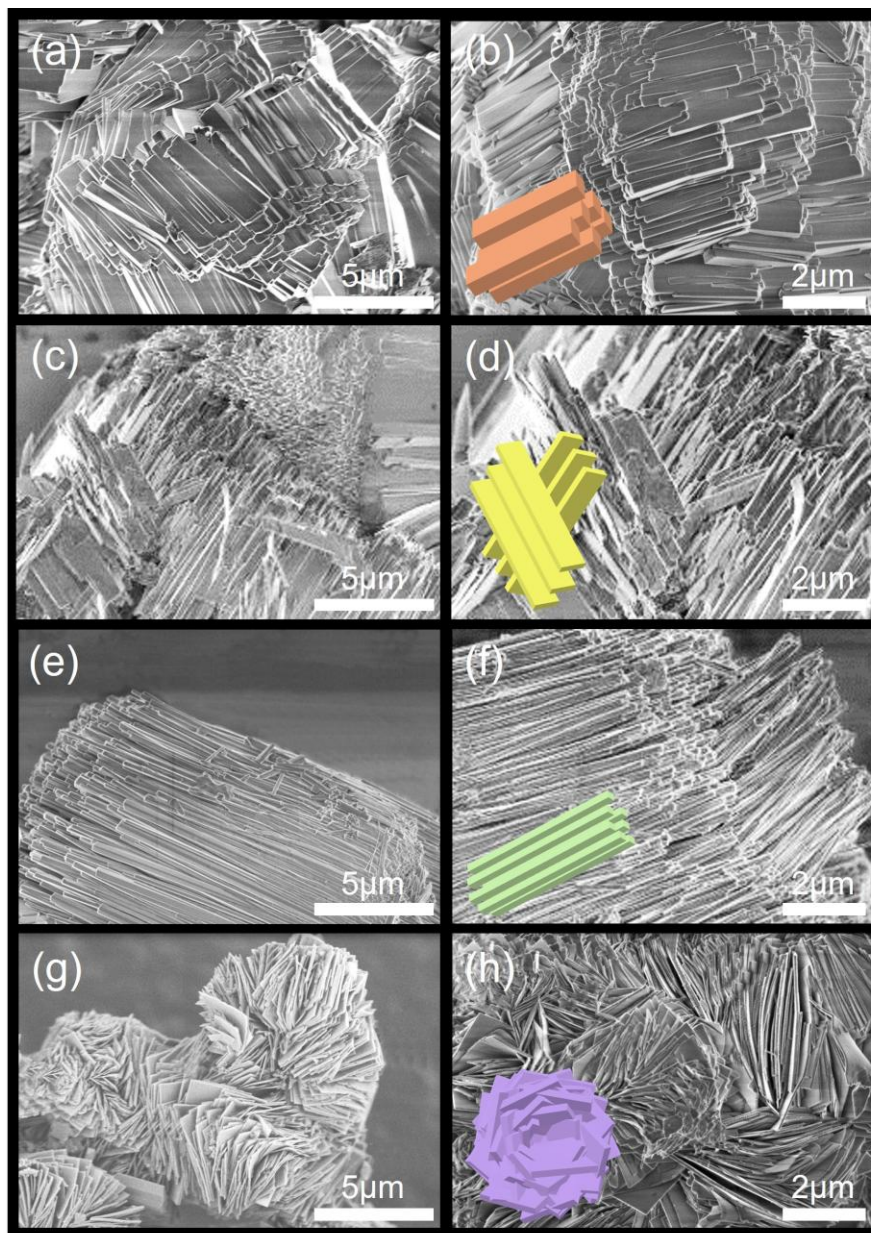


Fig. 2: FESEM images of (a, b) pristine mordenite, (c, d) TM-0.2, (e, f) TM-0.3 and (g, h) TM-0.4.

Table 1. Properties of pristine and hierarchical mordenite samples.

Samples	Si/Al ratio ^a	S_{BET}	S_{micro}	S_{ext}	V_{meso}	V_{Tot}	D_{av}	TPD-NH ₃ acidity (mmol/g)			
		(m ² /g) ^b	(m ² /g) ^c	(m ² /g) ^d	(cm ³ /g) ^e	(cm ³ /g) ^f	(nm) ^g	Weak	Medium	Strong	Total
Mordenite	6.10 (6.14)	449	435	13	0.09	0.24	5.1	0.62	1.13	0.29	2.04
TM-0.2	6.52 (6.70)	426	392	34	0.14	0.27	6.8	0.23	1.32	0.28	1.83
TM-0.3	6.74 (6.79)	411	365	46	0.17	0.28	8.3	0.20	1.21	0.30	1.70
TM-0.4	7.01 (7.07)	90	2	88	0.11	0.11	4.8	0.15	0.12	0.08	0.35

^aCalculated from XRF and ²⁹Si NMR (in bracket); ^bTotal surface area; ^cmicropore surface area; ^dexternal surface area; ^emesopore volume;

^fmesopore volume, ^gaverage pore size from BJH adsorption curve

IR spectroscopy, a very sensitive technique for analyzing the zeolite framework structure and functional groups [31], was employed to investigate the structural evolution of mordenite zeolite upon the incorporation of OTMS. Notably, TM-0.2 and TM-0.3 display a similar IR spectral pattern to pristine mordenite in the fingerprint region ($400\text{--}800\text{ cm}^{-1}$) (Fig. 3a–c), indicating a shared crystalline phase as proven by the XRD observations. The IR bands at 1229 and 1075 cm^{-1} correspond to Si–O–T (T = Si, Al) asymmetric stretching vibrations while their bending vibrations resonating at 564 cm^{-1} [32]. The existence of t-dah, t-kaj, t-mor and t-tes secondary building units (SBUs) for the MOR structure is signatred by the keen-edged peaks at 781 , 733 , 688 and 631 cm^{-1} , respectively [3]. Furthermore, a strong IR band at 453 cm^{-1} due to the tetrahedral TO_4 vibrations is also detected [33]. For TM-0.4, representing a mix-phase of ANA/GIS, exhibits a completely different IR spectral pattern (Fig. 3d). Nevertheless, all organosilane-functionalized samples show additional IR bands at 2860 and 2900 cm^{-1} (due to aliphatic CH_2 and CH_3 stretching), confirming the chemical incorporation of OTMS onto the aluminosilicate framework [34].

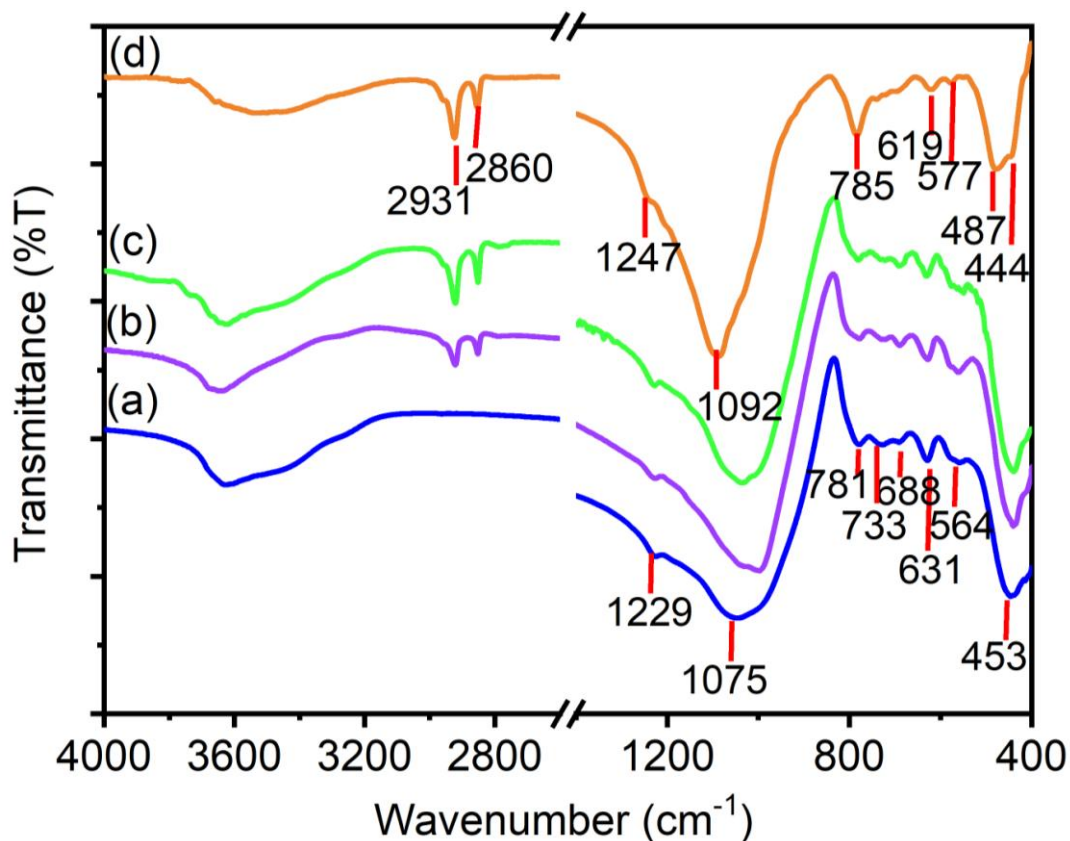


Fig. 3: IR spectra of (a) pristine mordenite, (b) TM-0.2, (c) TM-0.3 and (d) TM-0.4.

The incorporation of OTMS into the zeolite solids is further confirmed through the TG/DTG analysis where the TG/DTG profile of pristine mordenite is also recorded for comparison. Pristine mordenite shows two weight loss steps at 105 °C (7.5%) and 255 °C (2.1 %) due to the removal of physisorbed and chemisorbed water, respectively [35]. Upon the incorporation of OTMS, the modified samples show an additional weight loss at 280 °C, evidenced by an increasing DTG signal. The calculated OTMS contents in TM-0.2, TM-0.3 and TM-0.4 are 17.3, 21.6, 21.1 mmol/g solid, respectively, indicating that one OTMS molecule is enfolded by approximately 84, 66 and 69 TO₂ tetrahedra. In addition, it can also be seen that the

DTG signal at <200 °C is becoming weaker upon incorporation of OTMS indicating reduced amount of physisorbed water. This phenomenon could be explained by the increase of surface hydrophobicity as a result of the increased Si/Al ratio (Table 1). In addition, TM-0.4 shows narrower DTG signal in this region compared to other counterparts which can be explained by its ANA/GIS intergrown phase.

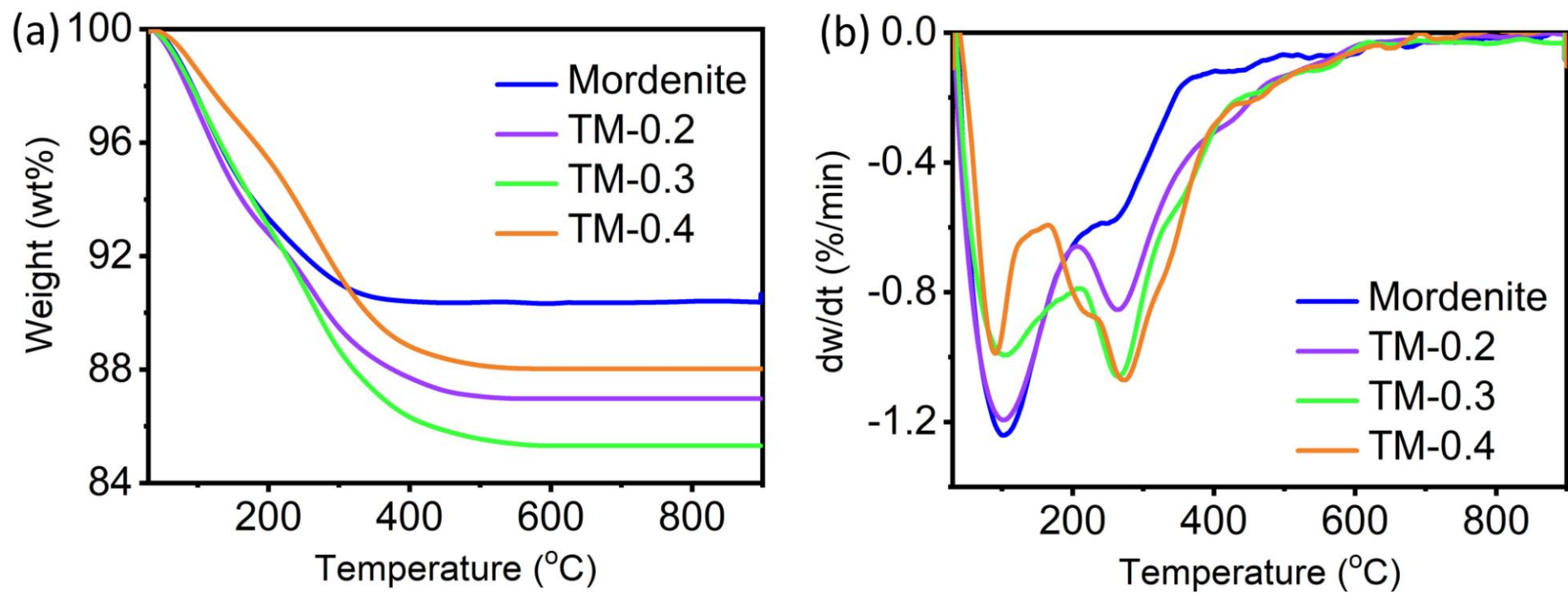


Fig. 4: (a) TG and (b) DTG curves of pristine mordenite, TM-0.2, TM-0.3 and TM-0.4.

^{29}Si CP MAS NMR spectroscopy is carried out to study the local chemical environment of Si atoms. For pristine mordenite, three deconvoluted NMR peaks appear at -113.6 , -103.6 and -98.6 ppm assigned to Q_4 (4Si, 0Al), Q_3 (3Si, 1Al) and Q_2 (2Si, 2Al) species, respectively [23] (Fig. 5a). Upon the incorporation of OTMS, these three peaks remain in TM-0.2 and TM-0.3 samples but are slightly shifted downfield (ca. -0.1 ppm) due to the higher Si/Al ratio; the Si atom is more electronegative than the Al atom (Fig. 5b,c). Apart from that, a weak signal due to T_3 ($(\text{OSi})_3\text{Si-R}$) species is detected at -71.6 ppm, confirming the presence of covalent bonding between OTMS and mordenite framework. This peak becomes more intense with increasing the OTMS/ Al_2O_3 ratio.

On the other hand, the T_2 peak is also observed in the ANA/GIS solid (TM-0.4), alongside the presence of four Q_n species, namely Q_4 (-111.5 ppm), Q_3 (-103.1 ppm) and two Q_2 (-98.5 , -93.9 ppm) (Fig. 5d). These four peaks are also slightly shifted compared to the mordenite sample because of the different framework structure that contributes to the different local chemical environment [36].

The deconvoluted peaks are also used to compute the Si/Al ratio of mordenites using Equation 1. It is found that the calculated Si/Al ratios for pristine mordenite, TM-0.2, TM-0.3 and TM-0.4 are 6.14, 6.70, 6.79 and 7.07, respectively, matching well with the XRF spectroscopy results (Table 1).

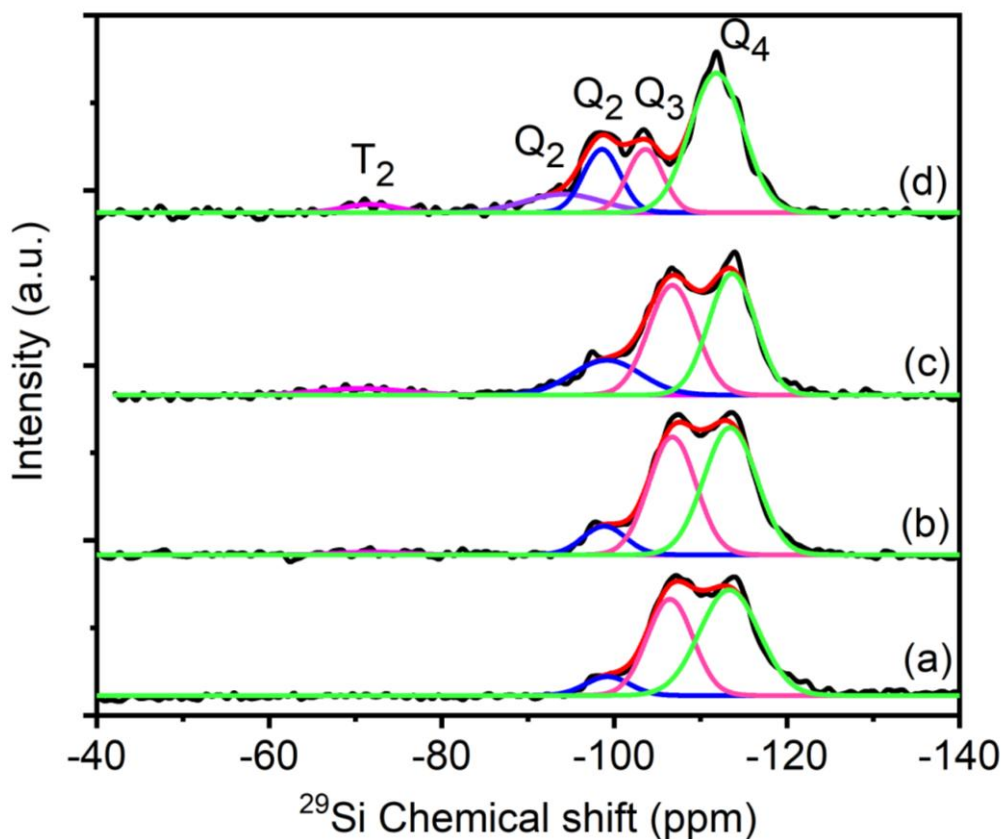


Fig. 5: ^{29}Si MAS NMR spectra of (a) pristine mordenite, (b) TM-0.2, (c) TM-0.3 and (d) TM-0.4.

The inclusion of OTMS mesoporegen during hydrothermal synthesis not only influences the crystallinity, morphology and phase purity of mordenites but impacts the porous characteristics of samples too. Thus, nitrogen sorption is carried out at $-196\text{ }^{\circ}\text{C}$. Pristine mordenite displays type I adsorption isotherm, indicating its microporosity (Fig. 6a) [37]. However, a hysteresis loop appears at $P/P_0 \approx 0.45$ in the isotherms of TM-0.2 and TM-0.3 samples while maintaining their Type I isotherm (Fig. 6b,c). Moreover, a further increase of nitrogen adsorption at $P/P_0 > 0.90$ attributed to capillary condensation in mesopores is observed. This indicates that the incorporation

of OTMS has introduced secondary mesoporosity in mordenite samples.

The N₂ adsorption data reveals that the total surface area of hierarchical mordenites (TM-0.2 and TM-0.3) is reduced which is ascribed to the decrease in micropore surface area per gram of solid. By incorporating OTMS mesoporegen, it is confirmed the presence of secondary mesoporosity in both solids has increased the average pore size (Table 1). Thus, the hierarchical mordenite zeolites (especially TM-0.3) show an increase in the external surface area, mesopore volume and total pore volume compared to the pristine mordenite. On the other hand, TM-0.4—an intergrown ANA/GIS—displays type III adsorption isotherm, confirming its non-porous structure (Fig. 6d) [38].

0.4 which has ANA/GIS intergrown feature, it shows a distinct acidity distribution and strength compared to the aforementioned three mordenite samples, with very low acid density attributed to its low surface area and dense crystalline phase.

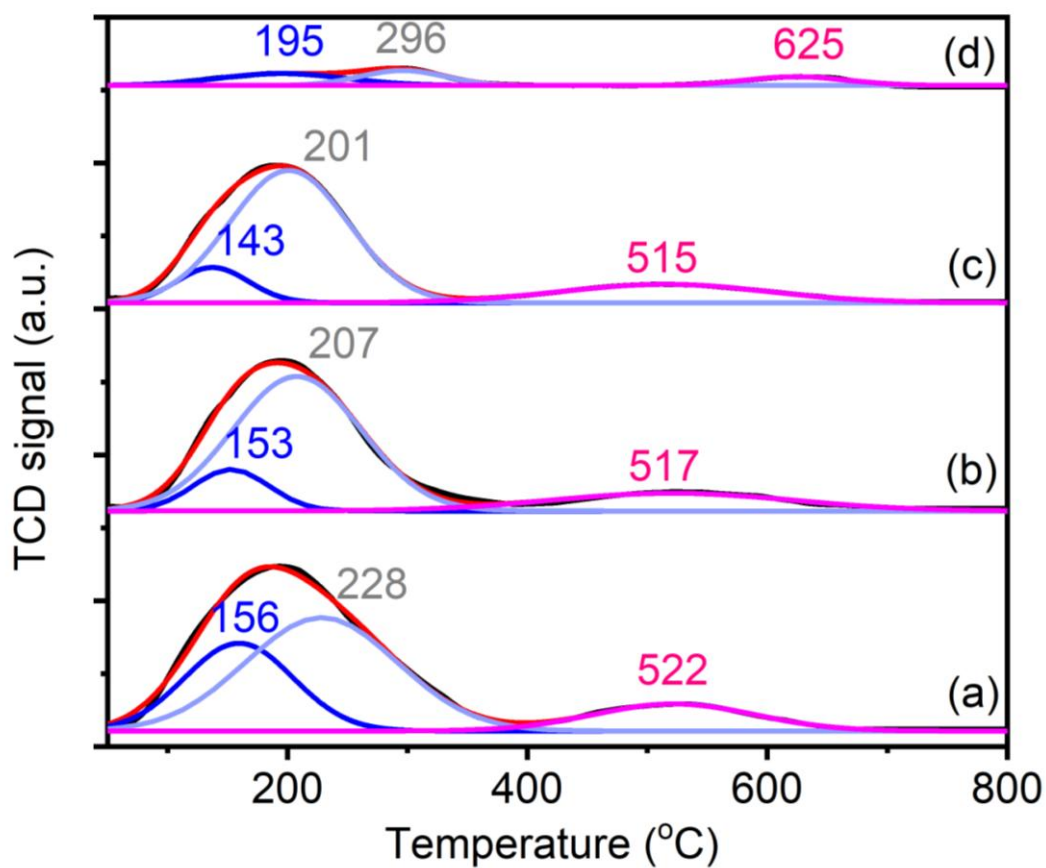


Fig. 7: TPD-NH₃ profiles of (a) pristine mordenite, (b) TM-0.2, (c) TM-0.3 and (d) TM-0.4.

3.2 Catalytic study

3.2.1 Catalytic study of hierarchical mordenites

Solvent-free acetalization of benzaldehyde and glycerol is chosen to evaluate

the catalytic behavior of mordenite catalysts, yielding two products, namely 2-benzyl-4-hydroxymethyl-1,3-dioxolane ($7.7 \times 6.2 \text{ \AA}^2$) and 2-benzyl-5-hydroxy-1,3-dioxane ($9.2 \times 4.8 \text{ \AA}^2$) (Fig. 8):

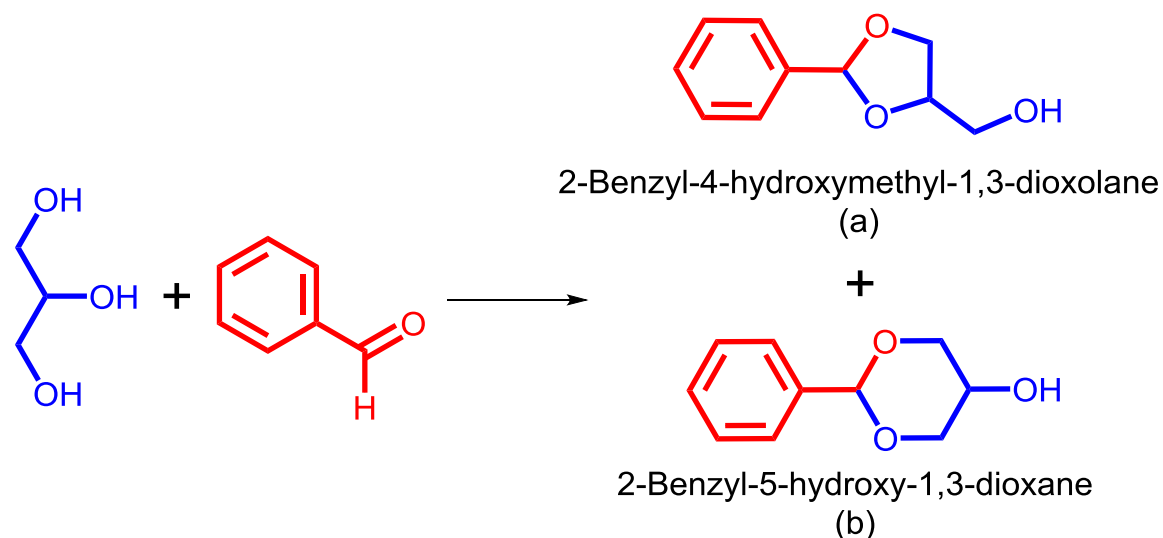


Fig. 8: Acetylation of benzaldehyde with glycerol yielding dioxolane and dioxane products.

The reaction is conducted at 120–160 °C for 0–60 min using non-microwave rapid heating. At 140 °C, low conversion (22.3%) is observed when no catalyst is added, even after 60 min, indicating that acetalization of glycerol is an activated reaction (Fig. 9A(a)) [39]. Additionally, the selectivity towards dioxolane and dioxane products is nearly 51:49 (Fig. 9B(a)). Nevertheless, the reaction conversion significantly increases (67.0–84.3%) after 60 min over mordenite catalysts where higher selectivity (62.3–67.1%) toward 2-benzyl-4-hydroxymethyl-1,3-dioxolane is achieved (Fig. 9A,B(b-c)). After 60 min onwards, the reaction reaches nearly equilibrium.

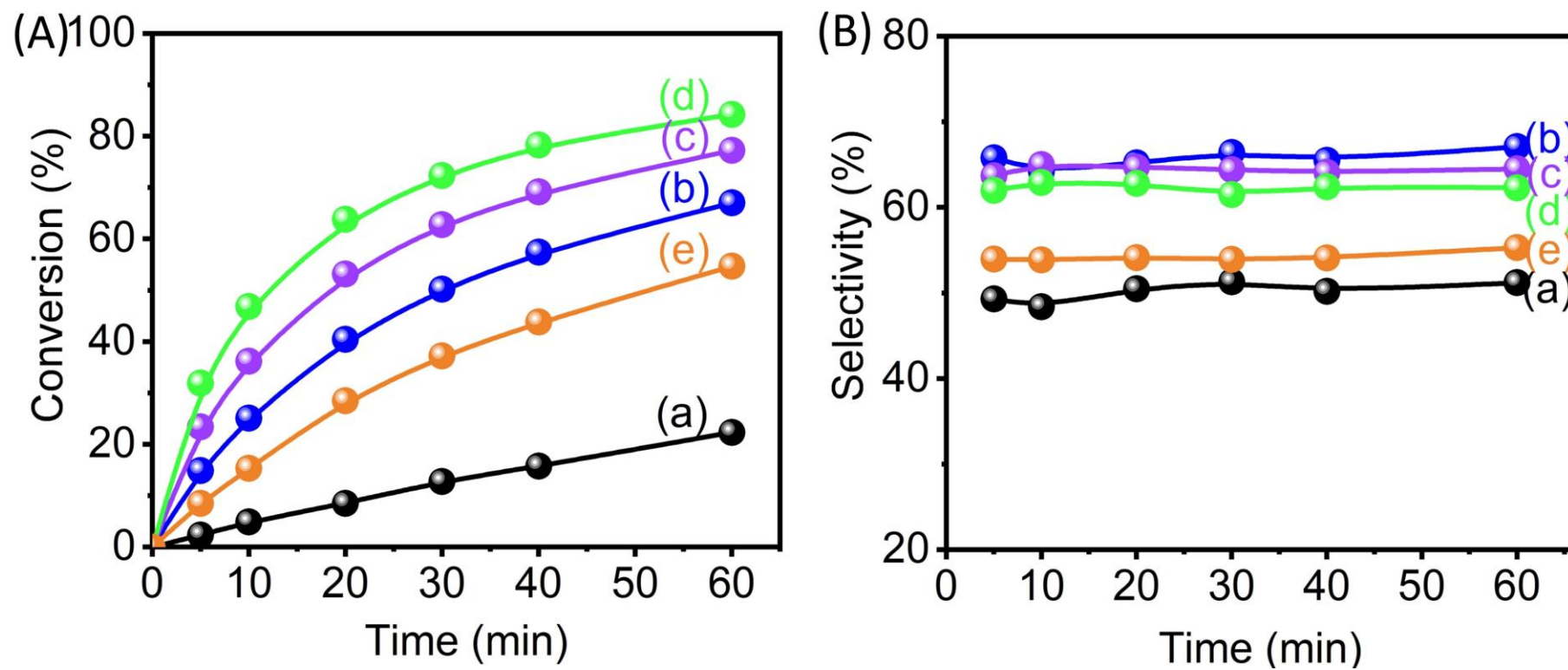


Fig. 9: (A) Reaction conversion and (B) dioxolane selectivity (a) without catalyst and (b) pristine mordenite, (c) TM-0.2, (d) TM-0.3 and (e) TM-0.4 at 140 °C. Catalyst loading = 0.050 g; benzaldehyde:glycerol molar ratio = 7:1; solvent-free.

The catalytic reaction findings also reveal the influence of zeolite morphology, porosity and crystalline phase on overall catalytic performance. TM-0.3 demonstrates the best catalytic performance (84.3% conversion, 62.3% selective to dioxolane), surpassing TM-0.2 (77.2%, 64.5%) and pristine mordenite (67.0%, 67.1%), respectively (Fig. 9). The high activity of TM-0.3 can be attributed to its largest average pore size (contributed by hierarchical mesoporosity) that facilitates high accessibility and diffusivity of reactants to the acid sites [40]. Although some glycerol and benzaldehyde molecules may access the micropores by positioning their conformation, the diffusion limitation, however, still can be expected especially in pristine mordenite. On the other hand, TM-0.4 as an intergrowth of ANA and GIS exhibits lower catalytic activity (54.7% conversion, 55.3% selective to dioxolane) than the mordenite counterparts due to its non-porous properties and low acid density (0.35 mmol/g) (Fig. 9A,B(d)). Its catalytic activity is mainly contributed by its secondary hierarchical mesoporosity.

To further understand the temperature-dependent relationship between reaction rates and catalysts, the activation energies (E_a) of acetylation of glycerol with and without catalysts are calculated using the Arrhenius equation [41]. The reaction was performed at 120, 140 and 160 °C for 60 min, and the Arrhenius linear graphs are plotted using the second order reaction rate constants. As shown, the reaction conversion increases drastically with temperature due to an increased kinetic energy factor (Fig. 10A). Notably, TM-0.3 shows the best reaction performance compared to other catalytic systems at 160 °C, where the high temperature increases effective

molecular collision frequency while the hierarchical porosity of TM-0.3 also facilitates the molecular diffusion to the active sites [42].

The non-catalyzed reaction displays a high activation energy (E_a) value of 100.8 kJ/mol due to the substantial energy required for activating the carbonyl oxygen of benzaldehyde (Fig. 10B(a)) [43]. However, the value significantly decreases to 91.6, 83.5, 78.4 and 96.3 kJ/mol in the presence of *pristine*, TM-0.2, TM-0.3, and TM-0.4 zeolite catalysts, respectively, where TM-0.3 displays the lowest E_a value (Fig. 10B(b–e)). This drastic reduction emphasizes the importance of acidic catalyst in acetylation of benzaldehyde, where large accessible hierarchical pores are complementarily essential for high molecular diffusion and accessibility.

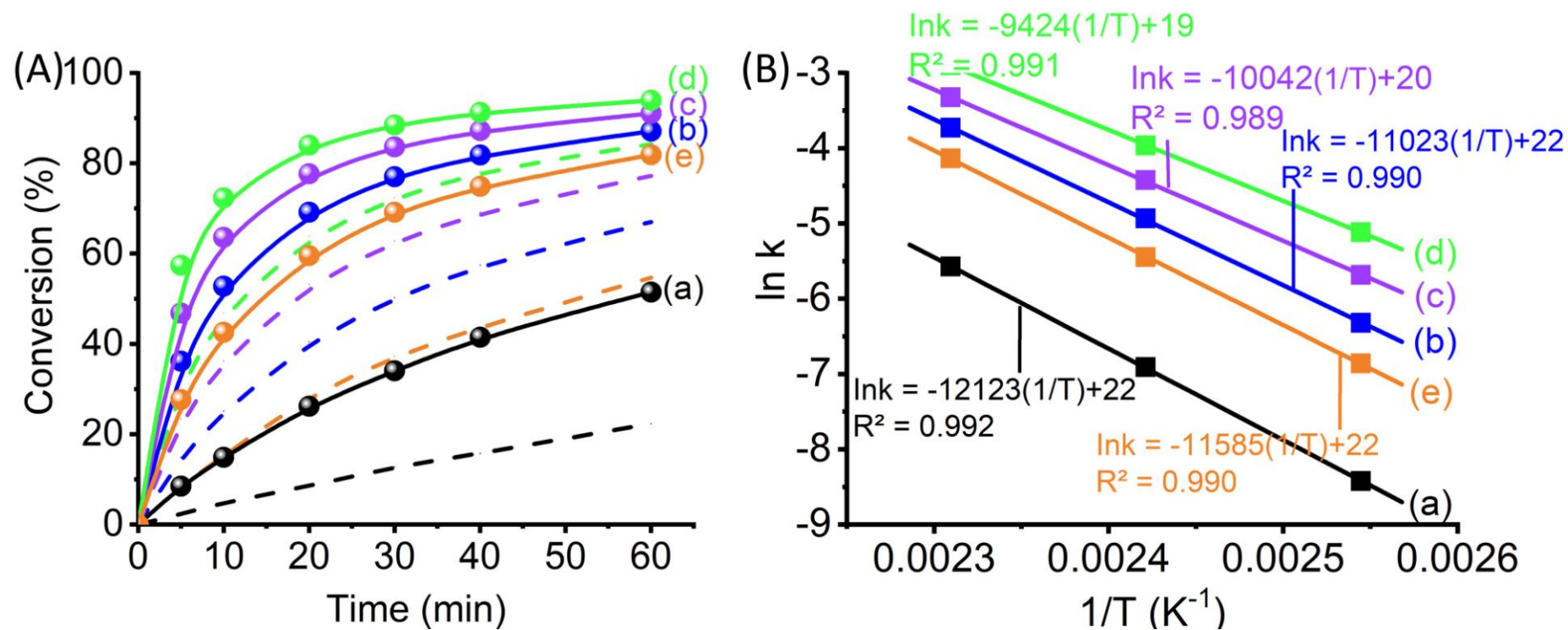


Fig. 10: (A) Effects of temperature on reaction conversion (a, black) without catalyst, and with (b, blue) pristine mordenite, (c, purple) TM-0.2, (d, green) TM-0.3 and (e, orange) TM-0.4 at 160 °C. Their respective conversion at 140 °C is shown in dashed curves. (B) Their respective Arrhenius linear plots using second order rate constants of 120, 140 and 160 °C. Catalyst loading = 0.050 g; benzaldehyde:glycerol molar ratio = 7:1; solvent-free.

Based on these results, the investigation of acetylation of benzaldehyde is further extended using the TM-0.3 hierarchical mordenite catalyst at 160 °C for 20 min since it gives the best catalytic performance (84.1% conversion, 62.8% selective to dioxolane). Parameters such as catalyst loading, molar ratio of benzaldehyde to glycerol, catalyst comparative study, and recyclability are explored in-depth.

3.2.2 *Effect of catalyst loading*

The effect of catalyst amount of TM-0.3 on the acetylation of benzaldehyde is studied at 160 °C for 20 min by varying the mass from 0 g until 0.200 g, while maintaining its glycerol to benzaldehyde molar ratio to 1:7. As anticipated, the conversion is minimal (26.2%) when no catalyst is added, reflecting the activated nature of the reaction (Fig. 11). However, as the catalyst amount increases, the reaction activity is enhanced, with the conversion increasing from 53.3% to 88.6% when the catalyst amount rises from 0.025 g to 0.100 g. This phenomenon is due to the increased number of acid sites that facilitate the occurrence of the reaction [44]. Meanwhile, the amount of catalyst does not influence the selectivity of dioxolane (ca. 61.5%). Nevertheless, further adding the catalyst amount causes inefficient stirring which leads to a drop in catalyst performance [45]. Hence the optimum loading of catalyst is 0.050 g since 0.100 g of catalyst shows almost similar catalytic activity.

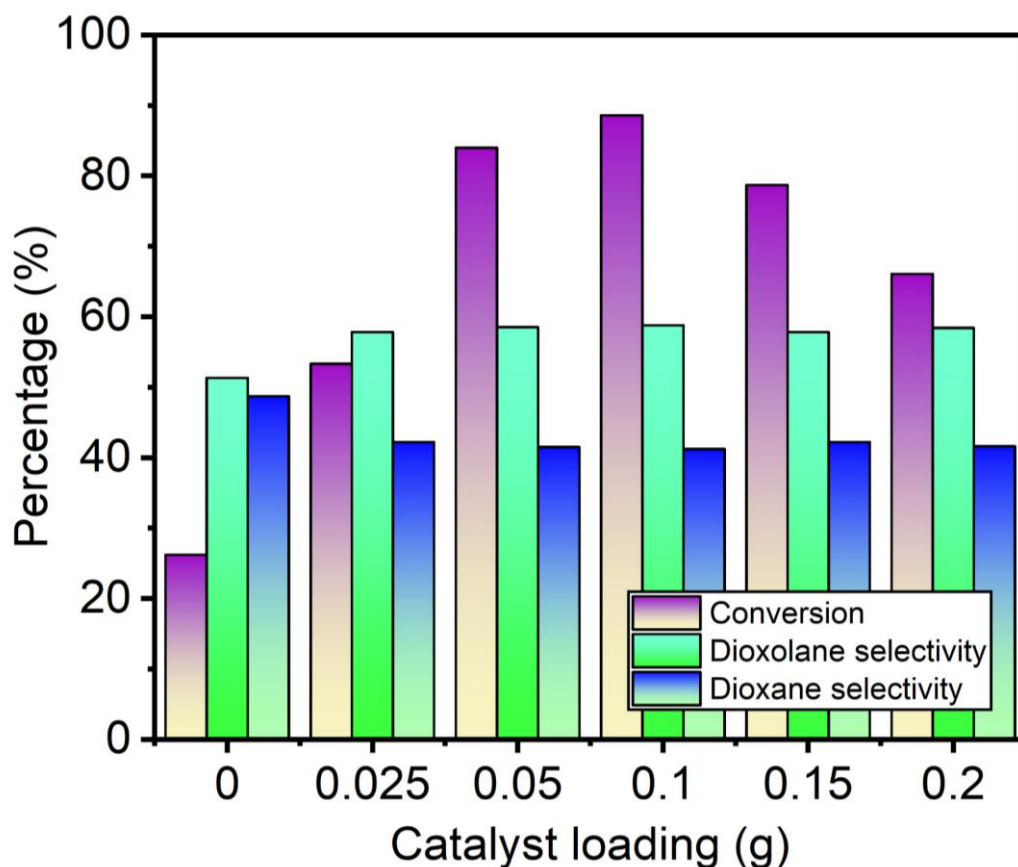


Fig. 11: Effect of catalyst loading on acetylation of benzaldehyde with glycerol. Temperature = 160 °C; time = 20 min; benzaldehyde:glycerol molar ratio = 7:1; solvent-free.

3.2.3 Effect of benzaldehyde:glycerol molar ratio

The molar ratio of reactants governs the behavior of a reaction since they directly take part in the reaction. Hence, acetylation reaction using different glycerol:benzaldehyde ratios of 1:1, 1:3, 1:5, 1:7, 3:1 and 7:1 is studied at 160 °C for 20 min in the presence of 0.050 g of TM-0.3 hierarchical zeolite catalyst. A remarkable increase in glycerol conversion is recorded, rising from 65.0% to 84.1%,

when the benzaldehyde concentration increases (from 1:1 to 1:7) (Fig. 12). This is because the limiting step in the reaction involves the protonation activation of carbonyl oxygen of benzaldehyde by the active sites of the catalyst [46]. On the other hand, when the glycerol is added in excess (from 1:1 to 7:1), the resulting mixture is becoming more viscous, causing difficulties in mixing and stirring; a gradual decline in the glycerol conversion from 65.1% to 47.8% is hence observed. Thus, this suggests that low amount of glycerol facilitates the homogenization of reactants which promotes acetylation reaction. Meanwhile, the selectivity of dioxolane remains nearly constant over varying the glycerol:benzaldehyde ratio, leveling at 61%. Thus, based on the results obtained, the optimum glycerol:benzaldehyde ratio is 1:7.

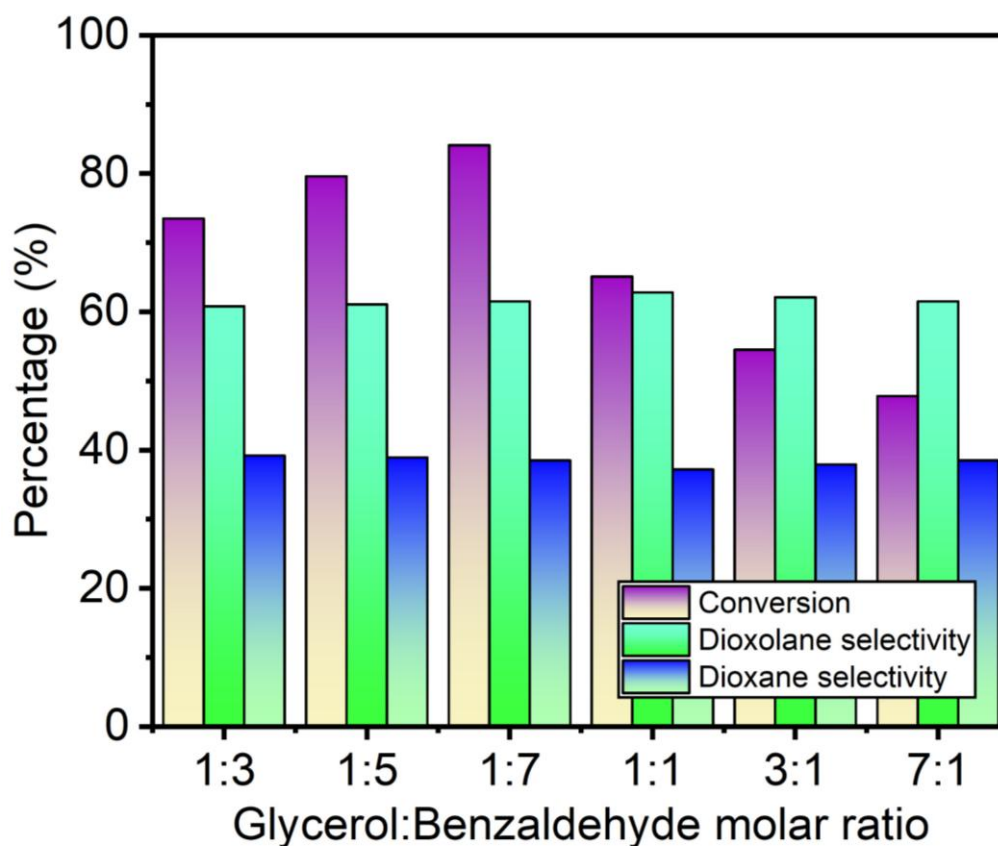


Fig. 12: Effect of glycerol:benzaldehyde ratio on acetylation of benzaldehyde with

glycerol. Temperature = 160 °C; time = 20 min; catalyst loading = 0.050 g; solvent-free.

3.2.4 Catalyst comparative study

The catalytic performance of hierarchical mordenite zeolite (TM-0.3) is compared with various classical homogeneous and heterogeneous catalysts at 160 °C for 20 min where the reaction conducted without a catalyst as a reference (conversion 26.2%, 52% selectivity of dioxolane) (Table 2, Entry 1). Strong concentrated acids such as hydrochloric acid and sulfuric acid achieve 100% benzaldehyde conversion but they suffer from very low selectivity towards dioxolane and dioxane; recording only 11.4% and 84.4% in total for both products, respectively (Entries 2–3). When weak acid such as acetic acid is applied, the catalyst is more selective to both dioxolane (59.0% selectivity) and dioxane (41.0 selectivity) products but the conversion is low (35.6%) (Entry 4).

Table 2: Catalytic performance of various catalysts on acetylation of benzaldehyde with glycerol producing (a) dioxolane and (b) dioxane products.

Entry	Catalyst	Conversion (%)	TON	TOF (s ⁻¹)	Selectivity (%)	
					(a)	(b)

1	No catalyst	26.2	–	–	51.3	48.7
2	H ₂ SO ₄	100	124.8	0.104	6.7	4.7
3	HCl	100	124.8	0.104	54.5	29.9
4	CH ₃ COOH	37.6	46.9	0.039	51.7	48.3
5	H-Y	52.7	65.8	0.055	58.2	41.8
6	H-LTL	56.2	70.1	0.058	60.2	39.8
7	Na-X	34.5	43.0	0.036	56.1	43.9
8	Na-A	30.4	37.9	0.032	57.9	42.1
9	MOR	69.1	86.2	0.072	63.9	36.1
10	TM-0.3	84.1	104.9	0.087	61.5	38.5
11	TM-0.3 (3 rd cycle)	82.2	102.6	0.085	61.0	39.0
12	TM-0.3 (5 th cycle)	78.5	97.9	0.082	61.2	38.8

*Catalyst loading = 17.4 μ mol equivalent to 0.050 g TM-0.3 solid;
benzaldehyde:glycerol molar ratio = 7:1; T = 160 °C; t = 20 min; solvent-free

Both acidic (H-Y and H-LTL) and basic (Na-X and Na-A) zeolites (pore size ranging from 0.41–0.74 nm) show lower activity (<34% conversion) compared to

hydrochloric acid and sulfuric acid which can be explained by their weaker acidity/basicity (Entries 5–8). However, these zeolite catalysts (56–59%) show better dioxolane selectivity than those homogeneous catalysts due to their molecular sieving effect [47]. When these zeolites are compared with the hierarchical mordenite zeolite, the latter catalyst outperforms the conventional zeolites, achieving 84.0% of conversion and 58.8% selective to dioxolane product (Entry 9). The exceptional catalytic performance of hierarchical mordenite is ascribed to its secondary mesoporosity that provides a larger pore size with more pore openings. Consequently, bulky reactants have better molecular mass transfer and increased accessibility to the active sites. Meanwhile, basic Na-A and Na-X zeolites (Si/Al = 1.0–1.2) shows poor catalytic activity compared to other acidic zeolites since acetylation is an acid-driven reaction.

Lastly, the TOF values on various catalysts are calculated to evaluate the catalytic efficiency besides providing insights into the reaction kinetics and performance of the catalysts (160 °C, 20 min) [48]. All the strong homogeneous acids show very high TOF (0.104 s^{-1}) revealing the catalytic ability of the acidic proton of strong acids (Entry 2–3). But they are corrosive and not recyclable. Meanwhile, TM-0.3 solid shows a TOF of 0.087 s^{-1} , which is the largest in those zeolite catalysts (TOF = $0.032\text{--}0.072\text{ s}^{-1}$), demonstrating that its acid sites are of high catalytic ability thanks to its hierarchical mesoporosity. Most importantly, this zeolite catalyst is recyclable where its TOF value only slightly drops to 0.085 and 0.084 s^{-1} after third and fifth cycles, respectively. Hence, hierarchical mordenite can be a promising catalyst for

chemical reactions involving bulky molecules for petrochemical and pharmaceutical industries. In addition, OTMS is also a promising mesopore agent for preparing hierarchical zeolites, which offers diverse opportunities to crystallize various molecular sieves with unique properties for advanced applications.

4. Conclusions

Octadecyltrimethoxysilane (OTMS) has been successfully used as a mesopore agent for synthesizing hierarchical mordenite. The optimum OTMS/Al₂O₃ ratio used for developing hierarchical structure is 0.3 (sample named TM-0.3) where further increasing the OTMS amount leads to the formation of intergrown ANA/GIS solid (TM-0.4). The resulting hierarchical mordenite exhibits nano-needle morphology with reduced micropore surface area and acid density but increased external surface area, mesopore volume and average pore size. Thanks to the secondary mesoporosity and accessibility of the pores, the modified mordenite catalyst is active in the acetylation of benzaldehyde with glycerol (84.1% conversion with 61.5% selectivity to dioxolane product) under **non-microwave** instant heating conditions (160 °C, 20 min). Furthermore, the catalytic performance is superior than of the pristine mordenite and other conventional homogeneous and zeolite-based catalysts. More importantly, the hierarchical mordenite catalyst produced using OTMS is reusable with insignificant loss in activity, offering it as a potential acid catalyst for chemical productions involving bulky molecules.

Declaration of competing interest

The authors have no competing interests to declare.

Acknowledgement

This work was funded by the USM Short-Term Grant (304/PKIMIA/6315725) and Princess Nourah bint Abdulrahman University, Saudi Arabia (Princess Nourah bint Abdulrahman University Researchers Supporting Project number PNURSP2024R47).

References

- [1] S.F. Wong, K. Deekomwong, J. Wittayakun, T.C. Ling, O. Muraza, F. Adam, E.P. Ng. Crystal growth study of K-F nanozeolite and its catalytic behavior in Aldol condensation of benzaldehyde and heptanal enhanced by microwave heating, *Mater. Chem. Phys.* 196 (2017) 295–301. <https://doi.org/10.1016/j.matchemphys.2017.04.061>.
- [2] G. Majano, E.P. Ng, L. Lakiss, S. Mintova. Nanosized molecular sieves utilized as an environmentally friendly alternative to antioxidants for lubricant oils. *Green Chem.* 13 (2011) 2435–2440. <https://doi.org/10.1039/C1GC15367F>.
- [3] IZA–SC, Database of zeolite structures. <http://www.izastructure.org/databases/> (Accessed 12 November 2023).

- [4] S. Narayanan, P. Tamizhdurai, V. L. Mangesh, C. Ragupathi, P. S. Krishnan, A. Ramesh. Recent advances in the synthesis and applications of mordenite zeolite – review. *RSC Adv.* 11 (2021) 250–267. <https://doi.org/10.1039/D0RA09434J>.
- [5] L. Xianfeng, R. Prins, J. Anton van Bokhoven. Synthesis and characterization of mesoporous mordenite. *J Catal.* 262 (2009) 257–265. <https://doi.org/10.1016/j.jcat.2009.01.001>.
- [6] M. Rilyanti, R.R. Mukti, G.T.M. Kadja, M. Ogura, H. Nur, E.P. Ng, Ismunandar. On the drastic reduction of organic structure directing agent in the steam–assisted crystallization of zeolite with hierarchical porosity. *Microporous Mesoporous Mater.* 230 (2016) 30–38. <https://doi.org/10.1016/j.micromeso.2016.04.038>.
- [7] P.S. Wheatley, P. Chlubná-Eliášová, H. Greer, W. Zhou, V.R. Seymour, D.M. Dawson, S.E. Ashbrook, A.B. Pinar, L.B. McCusker, M. Opanasenko, J. Čejka, R.E. Morris. Zeolites with Continuously Tuneable Porosity. *Angew. Chem. Int. Ed.* 53 (2014) 13210–13214. <https://doi.org/10.1002/anie.201407676>.
- [8] K. Zhang, M.L. Ostraat. Innovations in hierarchical zeolite synthesis. *Catal. Today.* 264 (2016) 3–15. <https://doi.org/10.1016/j.cattod.2015.08.012>.
- [9] E.P. Ng, L. Delmotte, S. Mintova. Environmentally benign synthesis of nanosized aluminophosphate enhanced by microwave heating. *Green Chem.* 10 (2008) 1043–1048. <https://doi.org/10.1039/B806525J>.
- [10] Q. Zhengxing, G. Jean-Pierre, V. Valtchev. Mesoporous zeolites by fluoride etching. *Curr. Opin. Chem. Eng.* 8 (2015) 1–6. <https://doi.org/10.1016/j.coche.2015.01.002>.

- [11] H. Koshti, M. Bandyopadhyay, R. Bandyopadhyay. Post-synthetically modified hierarchical Mordenite and ZSM-5 zeolite and their catalytic performances in benzylation of acetic acid to benzyl acetate. *J. Mater. Sci.* 58 (2023) 11914–11936. <https://doi.org/10.1007/s10853-023-08770-3>.
- [12] H. Koshti, R. Bandyopadhyay. Liquid-phase benzylation of toluene by benzyl alcohol over micro-mesoporous hierarchical mordenite zeolite. *Environ. Sci. Pollut. Res.* (2023). <https://doi.org/10.1007/s11356-023-26777-w>.
- [13] H. Koshti, M. Bandyopadhyay, M. Kumar, N.mTsunoji, R. Bandyopadhyay. Alkylation of Toluene to Mono-benzylated Toluene over Micro-mesoporous Zeolite: Effect of Post-synthetic Treatment and Catalytic Application. *Eur. J. Inorg.* 27 (2023) e202300674. <https://doi.org/10.1002/ejic.202300674>.
- [14] A. Feliczak-Guzik. Hierarchical zeolites: Synthesis and catalytic properties. *Microporous Mesoporous Mater.* 259 (2018) 33–45. <https://doi.org/10.1016/j.micromeso.2017.09.030>.
- [15] Z. Ke, S. Fernandez, T.O.B. Jeremy, T. Pilyugina, S. Kobaslija, M.L. Ostraat. Organotemplate-free synthesis of hierarchical beta zeolites. *Catal. Today.* 316 (2018) 26–30. <https://doi.org/10.1016/j.cattod.2017.11.033>.
- [16] Z. Kake, Egeblad. Kresten, C.H. Christensen. Mesoporous carbon prepared from carbohydrate as hard template for hierarchical zeolites. *Eur. J. Inorg.* 2007 (2007) 3955–3960. <https://doi.org/10.1002/ejic.200700218>.
- [17] C. Jo, J. Jung, H.S. Shin, J. Kim, R. Ryoo. Capping with multivalent surfactants for zeolite nanocrystal synthesis. *Angew. Chem. Int. Ed.* 52 (2013) 10014–10017.

<https://doi.org/10.1002/anie.201303088>.

- [18] S.M. Aleid Ghadah, F. Khoerunnisa, S. Rigolet, T. J. Daou, T.C. Ling, E.P. Ng. Hierarchical Cs-Pollucite Nanozeolite Modified with Novel Organosilane as an Excellent Solid Base Catalyst for Claisen–Schmidt Condensation of Benzaldehyde and Acetophenone. 8 (2020) 96. <https://doi.org/10.3390/pr8010096>.
- [19] Y.P. Guo, H. J. Wang, Y.J. Guo, L.H. Guo, L.F. Chu, C.X. Guo. Fabrication and characterization of hierarchical ZSM-5 zeolites by using organosilanes as additives. Chem. Eng. J. 166 (2011) 391–400. <https://doi.org/10.1016/j.cej.2010.10.057>.
- [20] E.P. Ng, J.H. Chow, R.R. Mukti, O. Muraza, T.C. Ling, K.L. Wong. Hydrothermal synthesis of zeolite a from bamboo leaf biomass and its catalytic activity in cyanoethylation of methanol under autogenic pressure and air conditions. Mater. Chem. Phys. 201 (2017) 78-85. <https://doi.org/10.1016/j.matchemphys.2017.08.044>.
- [21] Y.W. Cheong, S. Rigolet, T.J. Daou, K.L. Wong, T.C. Ling, E.P. Ng. Crystal growth study of nanosized K-MER zeolite from bamboo leaves ash and its catalytic behaviour in Knoevenagel condensation of benzaldehyde with ethyl cyanoacetate. Mater. Chem. Phys. 251 (2020) 123100. <https://doi.org/10.1016/j.matchemphys.2020.123100>.
- [22] E.P. Ng, J.H. Chow, S.F. Wong, R.R. Mukti, O. Muraza, T.C. Ling, K.L. Wong. Alkali Metal Ion-Exchanged Zeolite X from Bamboo Leaf Biomass as Base Catalysts in Cyanoethylation of Methanol Enhanced by Non-Microwave Instant

- Heating. Aust. J. Chem. 70 (2017) 1239-1246. <https://doi.org/10.1071/CH17168>.
- [23] G. Engelhardt, U. Lohse, V. Patzelová, M. Mägi, M. Mägi, E. Lippmaa. High resolution ^{29}Si n.m.r. of dealuminated Y-zeolites 1. The dependence of the extent of dealumination on the degree of ammonium exchange and the temperature and water vapour pressure of the thermochemical treatment. Zeolites. 3 (1983) 233–238. [https://doi.org/10.1016/0144-2449\(83\)90013-1](https://doi.org/10.1016/0144-2449(83)90013-1).
- [24] J.N. Appaturi, T. Pulingam, J.R. Rajabathar. Acid-base bifunctional SBA-15 as an active and selective catalyst for synthesis of ethyl α -cyanocinnamate via Knoevenagel condensation. Microporous Mesoporous Mater. 320 (2021) 111091. <https://doi.org/10.1016/j.micromeso.2021.111091>.
- [25] J. Nelson Appaturi, R. Jothi Ramalingam, M. Selvaraj, C. Stephen, T.S. Huat, F. Khoerunnisa, T.C. Ling g, E.P. Ng. Selective synthesis of triacetyl glyceride biofuel additive via acetylation of glycerol over NiO-supported TiO_2 catalyst enhanced by non-microwave instant heating. Appl. Surf. Sci. 545 (2021) 149017. <https://doi.org/10.1016/j.apsusc.2021.149017>.
- [26] J. Hagen. Industrial Catalysis: A Practical Approach, Second Edition, Wiley-VCH Verlag GmbH & Co, Germany: Weinheim. 1–8.
- [27] M.Y. Choo, J.C. Juan, L.E. Oi, T.C. Ling, E.P. Ng, A.R. Noorsaadah, C. Gabriele, K.T. Lee. The role of nanosized zeolite Y in the H_2 -free catalytic deoxygenation of triolein. Catal. Sci. Technol. 9 (2019) 772–782. <https://doi.org/10.1039/C8CY01877D>.
- [28] M.A. Hisham, E. Moustafa, E.A. Abdelrahman. Synthesis of mordenite zeolite in

absence of organic template. *Adv. Powder Technol.* 23 (2012) 757–760.

<https://doi.org/10.1016/j.appt.2011.10.003>.

- [29] S.S. Poly, S.M.A. Hakim Siddiki, A.S. Touchy, S. Yasumura, T. Toyao, Z. Maeno, K. Shimizu. High-silica H β zeolites for catalytic hydration of hydrophobic epoxides and alkynes in water. *J Catal.* 368 (2018) 145-154.
<https://doi.org/10.1016/j.jcat.2018.10.004>.

- [30] Y.K. Ma, S. Chia, T. J. Daou, F. Khoerunnisa, M.E.B. Salah, M.E.B. Zeinhom, T.C. Ling, E.P. Ng. SAPO-34 crystallized using novel pyridinium template as highly active catalyst for synthesis of ethyl levulinate biofuel. *Microporous Mesoporous Mater.* 333 (2022) 111754.
<https://doi.org/10.1016/j.micromeso.2022.111754>.

- [31] M. Yik-Ken, S. Rigolet, L. Michelin, J.L. Paillaud, S. Mintova, F. Khoerunnisa, T.J. Daou, E.P. Ng. Facile and fast determination of Si/Al ratio of zeolites using FTIR spectroscopy technique. *Microporous Mesoporous Mater.* 311 (2021) 110683. <https://doi.org/10.1016/j.micromeso.2020.110683>.

- [32] S.F. Wong, H. Awala, A. Vincente, R. Retoux, T.C. Ling, S. Mintova, R.R. Mukti, E.P. Ng. K-F zeolite nanocrystals synthesized from organic-template-free precursor mixture. 249 (2017) 105–110.
<https://doi.org/10.1016/j.micromeso.2017.04.053>.

- [33] T. M. Ali Ghrear, S. Rigolet, T. J. Daou, S. Mintova, T.C. Ling, S.H. Tan, E.P. Ng. Synthesis of Cs-ABW nanozeolite in organotemplate-free system. *Microporous Mesoporous Mater.* 277 (2019) 78–83.

<https://doi.org/10.1016/j.micromeso.2018.10.014>.

- [34] J. Clayden, N. Greeves, S. Warren. Organic Chemistry, Second edition, London: Oxford University Press (2012).
- [35] E.P. Ng, L. Delmotte, S. Mintova. Selective Capture of Water Using Microporous Adsorbents to Increase the Lifetime of Lubricants. *ChemSusChem*. 2 (2009) 255–260. <https://doi.org/10.1002/cssc.200800234>.
- [36] I. Hannus, A. Fonseca, I. Kiricsi. ^{29}Si and ^{27}Al MAS NMR investigation of H-mordenite dealuminated with phosgene. *Stud. Surf. Sci. Catal.* 94 (1995) 155–162. [https://doi.org/10.1016/S0167-2991\(06\)81217-6](https://doi.org/10.1016/S0167-2991(06)81217-6).
- [37] J.A. Delgado, M.A. Uguina, J.M. Gómez. Adsorption equilibrium of carbon dioxide, methane and nitrogen onto Na- and H-mordenite at high pressures. *Sep. Purif. Technol.* 48 (2006) 223–228. <https://doi.org/10.1016/j.seppur.2005.07.027>.
- [38] M. Fukuda, T. Onizuka, H. Tokumaru, H. Horikoshi, T. Iwasaki. Synthesis of NaP1 zeolite from silica waste as an absorbent for the removal of Cs^+ and Sr^{2+} from aqueous solution. *Chem. Eng. Res. Des.* 200 (2023) 706–715. <https://doi.org/10.1016/j.cherd.2023.11.038>.
- [39] J.R. Christopher. Zeolite Mediated Reactions: Mechanistic Aspects and Environmental Applications. *Prog. React. Kinet.* 33 (2008) 1–79. <https://doi.org/10.3184/146867807X272994>.
- [40] E. Koohsaryan, M. Anbia. Nanosized and hierarchical zeolites: A short review. *Chin. J. Catal.* 37 (2016) 447–467. [https://doi.org/10.1016/S1872-2067\(15\)61038-5](https://doi.org/10.1016/S1872-2067(15)61038-5).

- [41] J. Masa, S. Barwe, C. Andronesu, W. Schuhmann. On the Theory of Electrolytic Dissociation, the Greenhouse Effect, and Activation Energy in (Electro)Catalysis: A Tribute to Svante Augustus Arrhenius. *Chem. Eur. J.* 25 (2018) 158–166. <https://doi.org/10.1002/chem.201805264>.
- [42] E.P. Ng, H. Nur, K.L. Wong, M.N. Mohd Muhid, H. Hamdan. Generation of Brønsted acidity in AIMCM-41 by sulphation for enhanced liquid phase tert-butylation of phenol. *Appl. Catal. A: Gen.* 323 (2007) 58–65. <https://doi.org/10.1016/j.apcata.2007.02.001>.
- [43] L.U. Okonye, Y. Yao, R. Jianwei, X. Liu, D. Hildebrandt. A perspective on the activation energy dependence of the Fischer-Tropsch synthesis reaction mechanism. *Chem. Sci.* 265 (2023) 11859. <https://doi.org/10.1016/j.ces.2022.118259>.
- [44] H. Serafim, I.M. Fonseca, A.M. Ramos. Valorization of glycerol into fuel additives over zeolites as catalysts. *Chem. Eng. J.* 178 (2011) 291–296. <https://doi.org/10.1016/j.cej.2011.10.004>.
- [45] K. Ramachandran, T. Suganya, N. Nagendra Gandhi, S. Renganathan. Recent developments for biodiesel production by ultrasonic assist transesterification using different heterogeneous catalyst: A review. *Renew. Sust. Energ. Rev.* 22 (2013) 410–418. <https://doi.org/10.1016/j.rser.2013.01.057>.
- [46] F. Wang, S. Zhu, Q. Meng, H. Yin. Theoretical studies of nickel-catalyzed ring-opening hydroacylation of methylenecyclopropanes and benzaldehydes. *J. Mol. Model* 21 (2015) 203. <https://doi.org/10.1007/s00894-015-2754-6>.

- [47] G. Sastre, A. Corma. The confinement effect in zeolites. *J. Mol. Catal. A: Chem.* 305 (2009) 3–7. <https://doi.org/10.1016/j.molcata.2008.10.042>.
- [48] O. Celikbicak, G. Bayramoglu, M. Yılmaz, G. Ersoy, N. Bicak, B. Salih, M.Y. Arica. Immobilization of laccase on hairy polymer grafted zeolite particles: Degradation of a model dye and product analysis with MALDI–ToF-MS. *Microporous Mesoporous Mater.* 199 (2014) 57–65. <https://doi.org/10.1016/j.micromeso.2014.08.003>.